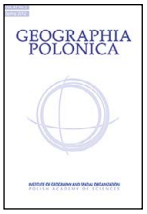

Geographia Polonica
2025, Volume 98, Issue 2, pp. 149-169
https://doi.org/10.7163/GPol.0297

INSTITUTE OF GEOGRAPHY AND SPATIAL ORGANIZATION
POLISH ACADEMY OF SCIENCES
www.igipz.pan.pl

www.geographiapolonica.pl

SURFACE TEMPERATURE EXTREMES IN URBAN AREAS: DISTRIBUTION, MORPHOLOGICAL DRIVERS AND AIR TEMPERATURE PATTERNS

Kaja Czarnecka

Institute of Geography and Spatial Organization, Climate Research Department
Polish Academy of Sciences
Twarda 51/55, 00-818 Warsaw: Poland
e-mail: czarnecka@twarda.pan.pl

Abstract

The expansion of cities, alongside increasing climate-related risks, requires a better understanding of urban thermal patterns for sustainable planning. This study identifies thermal hot and cold spots in Warsaw using 25 land surface temperature (LST) images (2002-2018), air temperature data from 21 sites, spatial development indicators, CORINE Land Cover, and local climate zones. Spatial autocorrelation (Getis-Ord Gi*) and correlation analyses reveal that LST extremes are related to land cover, spatial development, and city centre proximity. Cluster analysis highlights distinct seasonal and diurnal air temperature regimes in hot/cold spots, emphasizing the need for integrated approaches in urban climate research.

Keywords

cold spot • hot spot • land surface temperature • air temperature • land cover • local climate zones • spatial development

Introduction

Unique characteristics of urban climate are increasingly recognised as critical factors in city design and sustainability. As urbanised areas and their populations expand, comprehending the complex interactions between the built environment and local climate conditions is crucial for effective urban planning and management (Hebbert, 2014). The study of these compounds, along with the clear and accessible communication of their results to the public, is essential for transforming cities to be resilient to current and projected climate change (Oke, 2006).

The distinctive urban climate characteristics result from the landscape parameters, urban morphology, materials differed in albedo, heat storage and permeability, as well as anthropogenic sources of heat and air pollution, all of which interact with the regional climatic context (Oke, 1982; Kleerekoper et al., 2012; He et al., 2023; Czarnecka et al., 2024). These urban features significantly impact

local and large-scale ecological systems related to environment, health, and socioeconomics (Ai et al., 2024). One consequence is the formation of distinct thermal environments in cities, altering the frequency of thermally specific days and extreme phenomena such as heat and cold waves (Smid et al., 2019). Thermal conditions, even within the city limits, are notably uneven at different scales of analysis. An urban heat island is created on a city-wide scale – a general temperature gradient, with centres commonly warmer than suburban, less densely built-up areas (Oke, 1982; Kuchcik et al., 2024). However, when examining the thermal environment at finer spatial scales within the city, a more complex thermal mosaic emerges. Localized regions of significantly higher or lower land surface temperature can be identified, often forming spatially distinct clusters. These are referred to as thermal hot spots (THS) and thermal cold spots (TCS) (Mavrakou et al., 2018; Gupta, 2024). While the urban heat island effect is the subject of numerous scientific articles, the second phenomenon is less explored.

Thermal hot and cold spots (THCS) are commonly identified from land surface temperature (LST) images due to relatively good spatial resolution, broad coverage and high availability (Feyisa et al., 2016; Jamei et al., 2019; Lehnert et al., 2023). In urban climate studies focusing on THCS, Landsat products are the most commonly utilized (Guerri et al., 2022; Naserikia et al., 2023), although other satellite data such as Moderate Resolution Imaging Spectroradiometer (MODIS) (Grigoraș & Urițescu, 2018; Mavrakou et al., 2018) and Meteosat data (Sismanidis et al., 2017) are also employed. Other sources of information used for the detection of THCS on a much smaller scale are very high-resolution airborne thermal infrared remotely sensed data and semantically segmented longitudinal thermal images (Coutts et al., 2016; Ramani et al., 2024). The resolution and quality of these data are very high, however, the cost of acquiring, processing, and storing them is high, which means that they are not often used in urban research.

A similar principle applies to acquiring other parameters while investigating the details of the urban environment, which supports climate research. Satellite imagery is primarily utilised to calculate indicators related to spatial development – such as vegetation, built-up areas, surface types, and urban geometric composition (Jamei et al., 2019; Hidalgo-García & Arco-Díaz, 2022). Data from Light Detection and Ranging (LIDAR), urban databases and own inventory research are also used. Researchers often utilise various types of land categorisation to facilitate in-depth studies of landscape characteristics and enable comparison of results. This approach includes the use of numerous products with varying temporal and spatial resolutions, such as a regional CORINE Land Cover (CLC) inventory (Copernicus Land Monitoring Service, accessed: 3.09.2024), or a global map of local climate zones (Demuzere et al., 2022). A common approach is also to process satellite images independently to divide the area into self-selected land use/land cover types (Hussain et al., 2023).

Although the literature on the local climate is vast, there are still gaps in knowledge that need to be filled. There is a lack of comprehensive studies examining local thermal anomalies – both hot and cold – across various land cover types and local climate zones, not only those most commonly associated with them but also their relationship with urban morphology and thermal regimes. Therefore, this study aimed to (1) determine the elements of the urban environment associated with the formation of thermally distinctive surface spots and (2) their air temperature patterns. To reach this goal, the author detected thermal THS and TCS in Warsaw and then attempted to answer the following questions: What is the distribution of land surface temperature extremes in the city? What land cover types are associated with the occurrence of thermal hot and cold spots in urban areas? Does spatial development or distance from the city centre affect the occurrence of the spots? Is there a relationship between the frequency of the spots and thermal conditions?

What are the thermal regimes of areas where the spots appear? The research was carried out using both LST images and air temperature (AT) data. A better understanding of the functioning of THCS, considering the properties of both temperature-related parameters, may improve resilient urban planning and enable more accurate development of climate change mitigation strategies.

Study area

Warsaw is a dynamically evolving city with a diverse urban landscape located in east-central Poland, between latitudes 52°06' N and 52°22' N, longitudes 20°51' E and 21°16' E, with an area of 517.24 km^2(Office of Architecture and Spatial Planning of the Capital City of Warsaw City Hall, 2018; Statistics Poland, accessed: 14.08.2024). The elevation of Warsaw is from 74.8 to 152 m a.s.l, with an average of approximately 100 m a.s.l. The city is situated in the heartland of the Masovian Plain, on a moraine plateau, Pleistocene terraces and floodplains along the Vistula River. Its spatial development reflects a combination of dense urban cores, sprawling residential districts, road networks, greenery and blue infrastructure, all continuously expanding and becoming more concentrated. Between 2002 and the end of 2018, the population changed from 1,671,730 to 1,777,972 inhabitants. According to the Köppen–Geiger climate classification, Warsaw is located in either temperate oceanic (Cfb) or humid continental climate (Dfb), depending on the classification system used, due to its transitional nature (Peel et al., 2007; Rubel & Kottek, 2010). The climate is characterized by four distinct seasons, with warm summers and cold winters.

Material and methods

Identification of surface temperature extremes

The basis of the analysis consisted of 25 LST maps from 2002 to 2018, which are the outcome of the LIFE_ADAPTCITY_PL project (Tab. 1) (Dąbrowska-Zielińska et al., 2015, 2019). These products were processed from Landsat images with a resolution resampled to 30 m, whose transit time was between 9:00 and 9:30 a.m. UTC (+/– 15 min) (USGS, accessed: 31.07.2024). The authors of the maps performed atmospheric correction in the ATCOR v. 8.3.1 software, in which the influence of dust and aerosols in the atmosphere on the recorded values of reflected radiation was eliminated, as well as differences resulting from terrain unevenness.

In the following paper, the first step of the analysis was to exclude all surface water areas (the Vistula River, streams and reservoirs) and focus only on land properties. For this purpose, alongside the LST images, the Map of the Hydrographic Division of Poland by State Water Holding – Polish Waters and the Land functionality map of Warsaw 2019 provided by Warsaw City Council were utilised. Secondly, all acquired LST images converted to polygons were processed using the Optimized Hot Spot Analysis based on Getis-Ord Gi* statistic (Incident data aggregation method: count incidents within fishnet grid) in ArcMap 10.2.2. This tool utilizes the parameters derived from the characteristics of the input data to determine the settings that will yield the best hot/cold spot results, analyses the distribution of the weighted features and identifies the appropriate scale for analysis. Utilized spatial autocorrelation identifies hot and cold spots by calculating the degree to which high or low values are clustered within a specific distance from each data point. This paper defines features reflecting the confidence level at 95% and 99% as THS or TCS. The remaining pixels with LST values were named as areas where the effect did not occur – "no effect" (separately for hot and cold spots). Pixels without LST values at a given image (for example, due to cloud cover) were not subjected to Optimized Hot Spot Analysis and were defined as "no data".

The next stage was the creation of two maps – the frequency of THS and TCS. Twenty-five layers with attributes divided into

Table 1. Satellite imagery data and land surface temperature calculation algorithms

No	Satellite (sensor)	Dates	Algorithm to calculate land surface temperature
1 2 3 4 5 6 7	Landsat 5 (TM)	21.02.2002 13.09.2003 18.09.2005 21.09.2006 03.05.2007 19.05.2007 28.08.2009	$L = C_0 + C_1 \cdot DN$ $T_C = \left[\frac{K_2}{K_1 - \ln L}\right] - 273.15$ where: L – Spectral Radiance; C_0 and C_1 – radiometric calibration coefficients; DN – Digital Number value; K_1 and K_2 – the calibration constants (607.76, 1260.56).
8 9 10 11 12 13 14 15 16 17 18 19 20 21 22 23 24 25	Landsat 8 (OLI + TIRS)	19.05.2013 20.06.2013 08.09.2013 22.05.2014 23.04.2015 14.09.2015 02.04.2016 04.05.2016 05.06.2016 16.09.2016 05.04.2017 15.06.2017 28.09.2017 08.04.2018 15.04.2018 20.07.2018 30.08.2018 01.10.2018	$L_\lambda = M_L\, DN + A_L$ $T_C = \left[\frac{K_2}{\ln\left(\frac{K_1}{K_\lambda}\right) + 1}\right] - 273.15$ where: L – Spectral Radiance; M_L – Radiance Multiplier; DN – Digital Number value; A_L – Radiance Add; K_1 and K_2 – radiometric calibration factors (777.89, 1321.08).

Source: Based on Sameen & Kubaisy (2014) and Dąbrowska-Zielińska et al. (2015, 2019).

"THS" or "TCS", "no effect", and "no data" were superimposed. A value was calculated for each feature: the number of images when the effect appeared divided by the number of images where the feature was present (to exclude the influence of "no data") multiplied by 100. All areas where "no data" covered more than 50% of the images were excluded from the maps. As a result, 3.65% of Warsaw's area was eliminated from the analyses (surface water – 3.58%; missing pixels – 0.07%). Subsequently, the remaining data were divided into five frequency intervals, expressed as percentages: absent – 0.0%, sporadic – 0.1-25%, rare – 25.1-50.0%, frequent – 50.1-75% and very frequent 75.1-100%. The images used to create the THS and TCS maps came from different seasons, with none of the seasons accounting for more than 50% of the total number of images. Almost all images had less than 25% cloud cover (except for one image with less than 50%) and none of

the days were characterized by strong winds (IMGW-PIB, https://danepubliczne.imgw.pl/).

Comprehensive land cover-based analysis

To investigate which elements of the urban environment influence the formation of THCS, the first focus was on a comprehensive analysis – the frequency of occurrence of the effects in different land cover types. Two commonly applied classifications with complete datasets for the study area were selected.

The first part of the analysis was based on the CLC2000 and CLC2018 – detailed datasets on land cover for Europe with geometric accuracy of 50 m (CLC2000) or 10-15 m (CLC2018) and minimum mapping unit 25 ha, the use of which enabled focusing on the functional diversity of the area (Chief Inspectorate for Environmental Protection, accessed: 1.05.2024-a, 1.08.2024-b). CLC includes 44 thematic classes, divided into five main land cover types. Within the research area, 22 cover types were identified at level 3. '1. Artificial surfaces' accounted for a substantial 67.5%, with the subtype '112. Discontinuous urban fabric' is the most prominent. '3. Forest and semi-natural areas' made up 18.7% of the surface, with the subtype '312. Coniferous' is the most significant contributor. The remaining proportions of the research area consisted of '2. Agricultural areas' (11.2%), '5. Water bodies' (2.6%) and '4. Wetlands' (0.04%). For further analysis, surface water ('511. Water courses' and '512. Water bodies') was excluded to focus on the LST of land-related categories.

The second source was a global 100 m-resolution, high-accuracy LCZ map of data on urban features (Demuzere et al., 2022). The LCZ typology categorises urban (1-10) and natural (A-F) landscapes into 17 distinct types based on surface cover, structure, and thermal properties to analyse their impact on local climate and temperature patterns. The use of LCZ classification supplemented the analysis by providing information on various types of urban geometry and characteristics, even within areas of the same functionality, focusing on the influence of the physical characteristics of different kinds of development and land cover on the local climate. In Warsaw, 15 types of zones were identified within the research area. The dominant class was 'LCZ 5 Open midrise', covering 25.9%, followed by 'LCZ 6 Open lowrise' (23.0%) and 'LCZ A Dense trees' (19.7%). Each remaining type covered less than 10% of the research area. Only 'LCZ 8 Large lowrise', 'LCZ B Scattered trees' and 'LCZ D Low plants' occupied more than 5% of the surface. The remaining classes accounted for less than 15 km^2 each. The analysis excluded areas classified as surface water (LCZ G) to concentrate on the variation in thermal properties of land surfaces, focusing on the remaining 14 LCZ types.

For each map, an analysis of the frequency of THS and TCS effects was carried out, divided into CORINE Land Cover (CLC) categories and local climate zone (LCZ) types (Demuzere et al., 2023; Chief Inspectorate for Environmental Protection, accessed: 1.05.2024-a). To focus on the characteristics of specific land cover classes rather than the changes between 2002 and 2018, an "unchanged area" was marked out, which is referred to as the research area in this paper. This was achieved by utilizing the corrected CLC 2002 and CLC 2018 databases. Both CLC products were overlaid and combined, and only the attributes with matching land cover class codes were extracted, forming a key component of the analysis presented throughout this article. The delineated area serves as a "changed area" mask for the maps (Fig. 1) and then for both classifications considered in this study. The designated "unchanged area" constitutes 79.6% of Warsaw's total area.

Site-specific urban development and thermal condition analysis

The second part of the analysis focused on the selected sites differing in thermal conditions, proximity to the city centre, spatial arrangement, and THS or TCS frequency. These locations correspond to the monitoring

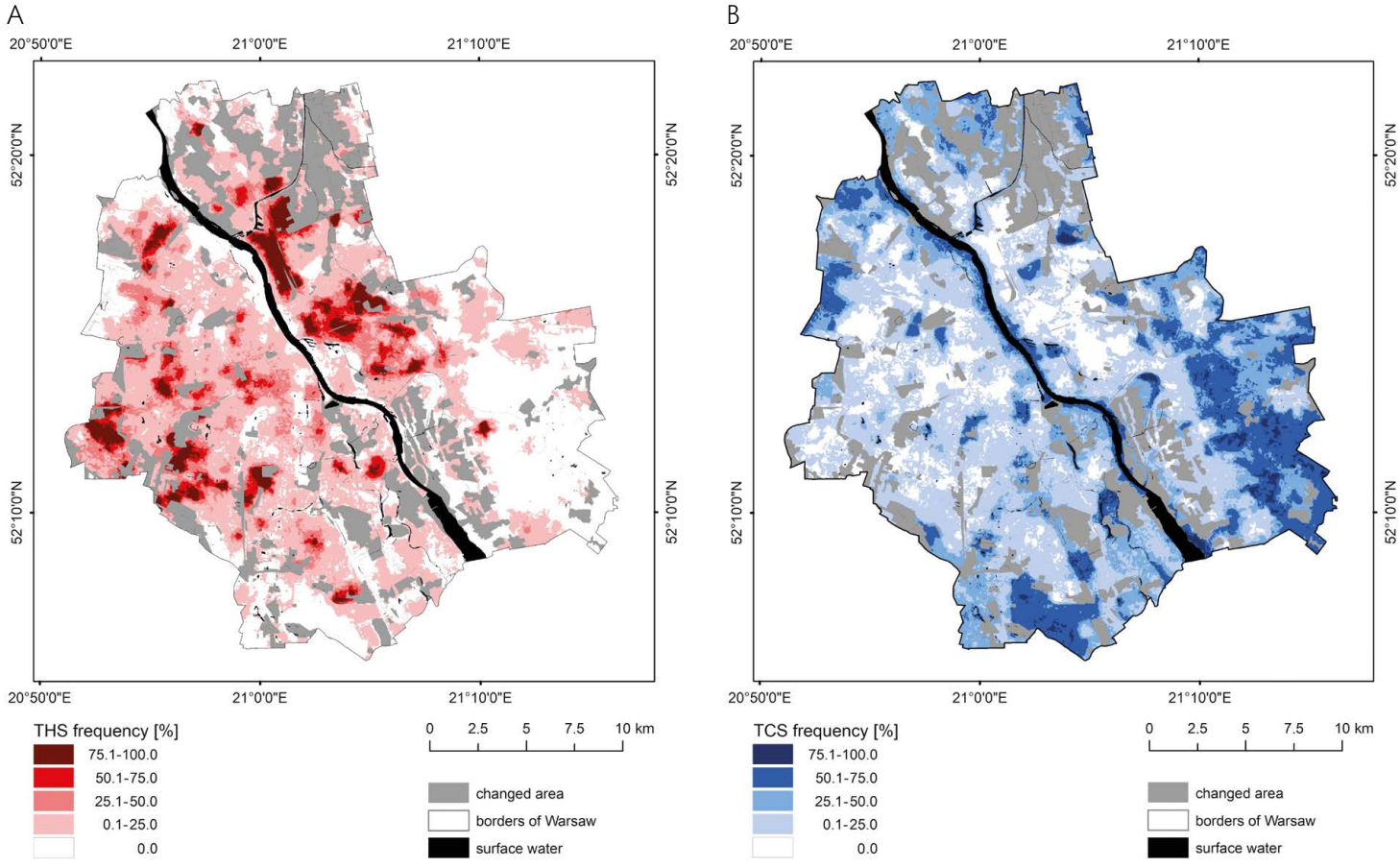

Figure 1. Frequency of thermal hot spot (A) and thermal cold spot (B) occurrence

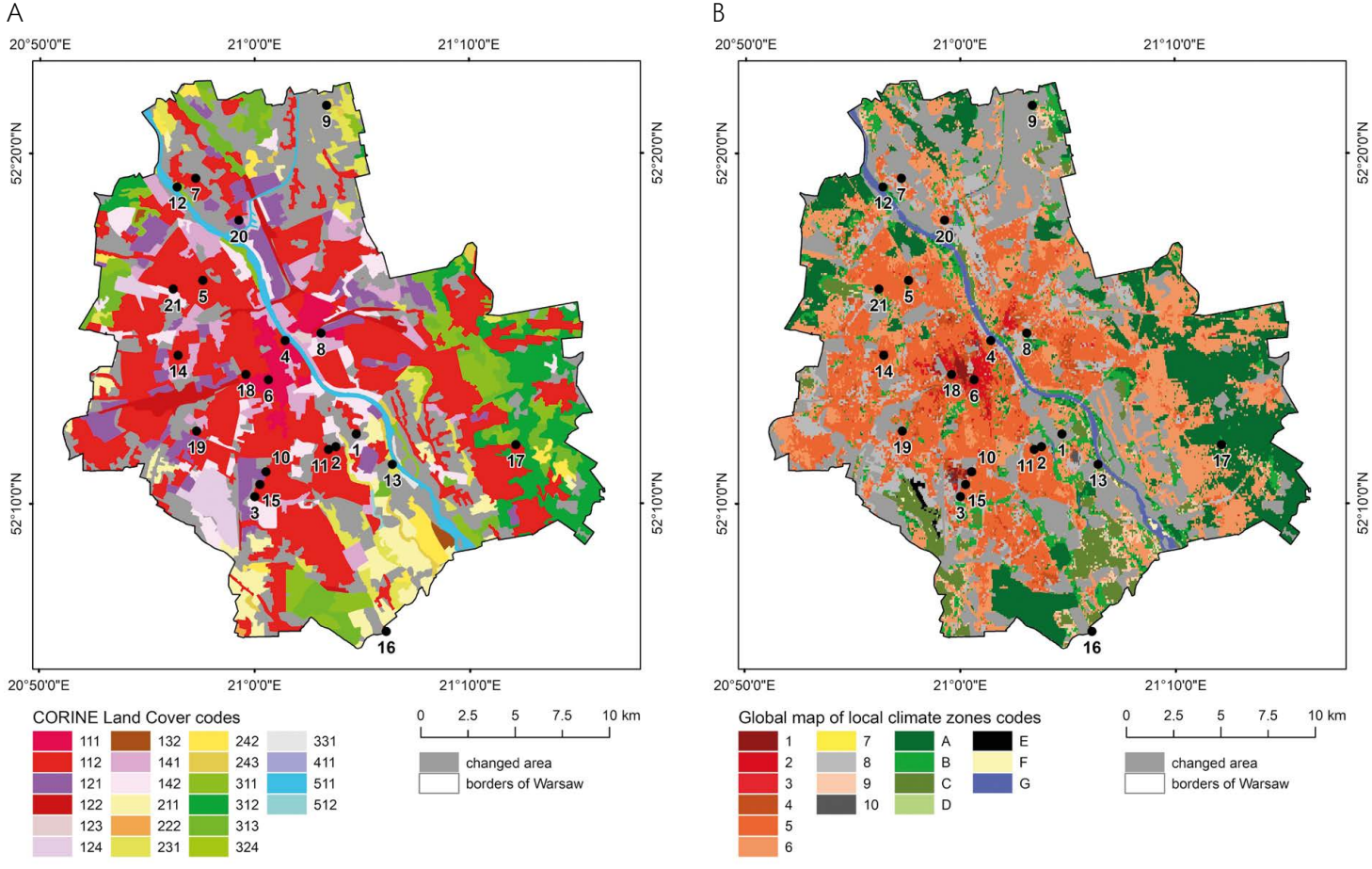

Figure 2. Location of measurement sites in the context of CORINE Land Cover

Source: (A) (Chief Inspectorate for Environmental Protection, accessed: 1.05.2024-a, 1.08.2024-b), and a global map of local climate zones (B) (Demuzere et al., 2023).

network of the Climate Research Department IGSO PAS. AT data from 21 loggers were utilised, covering the period from the network's expansion in 2009 to the study's end in 2018 (Fig. 2). At each site, a HOBO Pro U23-001 or U23-002 data logger (measuring range: -40 to 70°C; resolution: 0.04°C; accuracy±0.25°C from -40 to 0°C, ±0.2°C from 0 to 70°C) with a solar radiation shield was placed 2 meters above grassy surfaces, with a 10-minute logging interval.

Firstly, data on THS and TCS frequencies were extracted to analyse selected sites (Fig. 3). For THS, the average frequency was 18.8%, ranging from 0% (sites 3, 4, 12, 16, 17, 21) to 70.8% (site 10), while for TCS, the average was 17.7%, ranging from 0% (sites 6, 14, 18) to 65.2% (site 4).

Then, based on AT data, values of the average air temperature (AT_{avg}), the absolute minimum/maximum air temperature (AT_{abs_min}/AT_{abs_max}) and the average minimum/maximum air temperature (AT_{min}/AT_{max}) were calculated for each site.

Spatial development indicators for the measurement sites were sourced from Czarnecka et al. (2024) and validated using historical Google Earth Pro images, CLC2002, and CLC2018, focusing on non-overlapping research periods. These indicators, commonly applied in spatial planning, include vertical building characteristics (Maximum Building Height – BH_{max}; Mean Building Height – BH_{mean}), horizontal features (Building Coverage Ratio – BCR), combined dimensions (Floor Area Ratio – FAR) and a vegetation-related

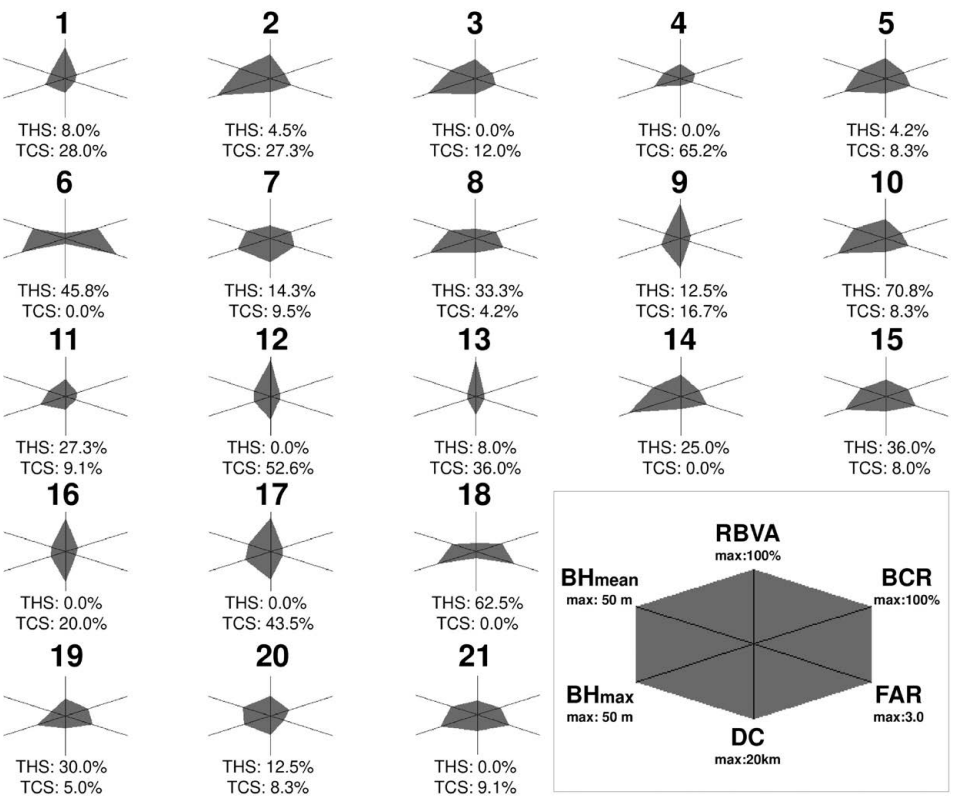

Figure 3. Characteristics of measurement sites – spatial development indicators, distance from the city centre and the frequency of THS and TCS occurrence

Source: Own elaboration based on Czarnecka et al. (2024).

metric (Ratio of Biologically Vital Area – RBVA) (Fig. 3). The sky view factor was excluded due to significant seasonal and interannual variability. Selected indicators were obtained for a 100m radius, as recommended for this type of research (Czarnecka et al., 2024). The distance from the city centre (DC), defined as Dmowski Roundabout, is expressed in kilometres. During the research period, the land cover (based on CORINE Land Cover) or spatial development within a radius of 100 m (spatial development indicators) did not change.

Statistical analysis was performed in the Statgraphic Centurion XVI v.16.2.04 software. To investigate whether there was a statistically significant correlation between the occurrence of THCS, spatial development indicators and the proximity from the city centre, Spearman's rank correlation (95% confidence level) was performed. A similar analysis was also conducted concerning the frequency of the phenomenon with selected thermal characteristics using annual AT data. The nonparametric measure was chosen due to the non-normal THS and TCS frequency data distributions across the analysed sites. To more accurately characterise areas with varying frequencies of THCS, hierarchical cluster analysis using Ward's minimum variance method (Euclidean distance) was performed based on THS and TCS (no strong outlier data). The number of clusters was limited by setting a threshold just below the largest increase in linkage distance, thus excluding grouping at 11.1 and the maximum distance of 17.1. The result was three distinct clusters, connected at the distance level of 4.4, 5.8 and 7.7 (Fig. 4). Each cluster was characterised by its centroids, AT characteristics, CLC category, LCZ type, spatial development indicators and DC mean values. Finally, for each cluster, AT values of all stations within it were averaged for each hour to present the daily regime for the whole year (I-XII), summer (VI-VIII) and winter (XII-II) separately.

Results

Spatial autocorrelation analysis showed that the locations where the THS occurred with a frequency above 50% exhibited a point-like pattern of varying sizes, concentrated on individual objects with exceptionally high land surface temperature compared to the surroundings (Fig. 1A). However, these areas covered a relatively small surface – 4.6% for the frequency range of 50.1-75% and 4.4% for the range of 75.1-100%. 100% frequency concerned for only 0.9% of the research area. A significantly larger surface – 43.1% – was characterised by sporadic occurrences of THS (0.1-25.0%), while 10.3% of the area showed a rare effect (25.1-50.0%). THS, which occurred at least once, covered 62.5% of the whole analysed area of the city, while the weighted mean of the frequency was 15.1%.

The distribution of the most frequent TCS effect took the form of extensive patches with distinct edges or elongated shapes along the Vistula River valley (Fig. 1B). The frequency range of 50.1-75% covered 17.1% of the research area, while 75.1-100.0% – 1.5%. The TCS 100% frequency did not occur. In the largest area – 44.0% – the effect occurred

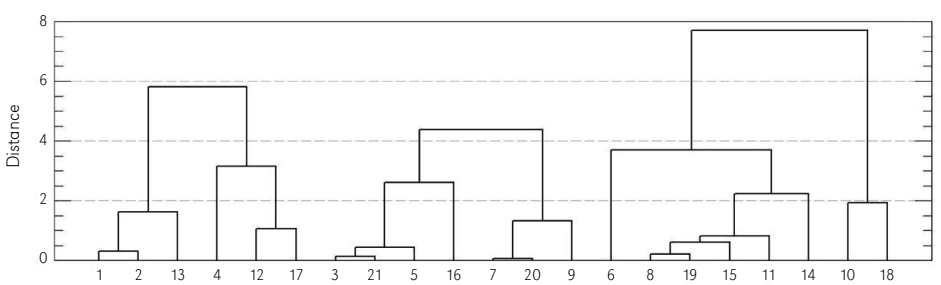

Figure 4. AT measurement sites in Warsaw clustered by THS and TCS frequencies

sporadically (0.1-25.0%), while it was rare (25.1-50.5%) in 21.7% of the surface. TCS, which occurred at least once, covered 84.4% of the analysed area with a 19.5% weighted mean of frequency.

Both phenomena were dispersed citywide, covering over half of the study area. THS and TCS overlapped 47.2% of the terrain, while exclusive THS and TCS areas covered 15.3% and 37.2%, respectively.

Impact of land cover and urban morphology on surface temperature extremes distribution

THS frequency analysis showed the phenomenon occurred in most categories, except '222. Fruit trees and berry plantations' (Fig. 5A). Among the remaining classes, the effect was either absent or sporadic (0.1-25.0%). The exception was '121. Industrial or commercial units' experienced occurrences of the effect with a frequency exceeding 75% on a dominant area of this subtype. Classes with very high THS occurrence were primarily artificial surfaces, excluding non-agricultural vegetated areas. The spatial variation in THS frequency was also analysed by examining the proportion of each category across different frequency ranges. Its distribution was closely related to the size of the area occupied by individual classes. '121. Industrial or commercial units' had the highest share in categories with frequent THS occurrences. In contrast, the whole area of THS frequency below 50% or without the effect was predominantly covered by '112. Discontinuous urban fabric'.

The TCS was observed across all land cover classes with a distribution pattern more varied than THS (Fig. 5B). Frequent TCS covered over half of forested areas (311, 312, 313), '411. Inland marshes' and '331. Beaches, dunes, sands', large portions of '243. Land principally occupied by agriculture, with significant areas of natural vegetation' and '141. Green urban areas'. Most other classes showed much lower TCS occurrence. The largest areas without TCS presence were found within the urban fabric classes (111, 112), '121. Industrial or commercial units' and '122. Road and rail networks and associated land'. When analysing the distribution of TCS frequencies within individual land cover classes, the category above 50% was dominated by three forest-related classes. The whole research area composed of the rarest occurrence of TCS, similar to THS, was associated with '112. Discontinuous urban fabric'.

The distribution of THS across areas occupied by various local climate zones was highly heterogeneous (Fig. 6A). The absence of the phenomenon covered the most extensive areas within categories 'LCZ 9 Sparsely built', 'LCZ A Dense trees', and 'LCZ B Scattered

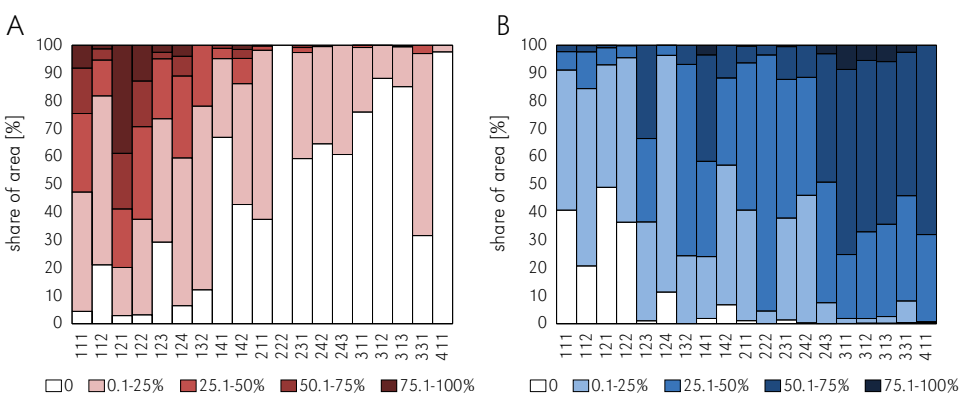

Figure 5. CORINE Land Cover categories in the research area, divided by the frequency ranges of THS (A) and TCS (B)

Legend source: According to https://clc.gios.gov.pl/doc/clc/CLC_Legend_EN.pdf

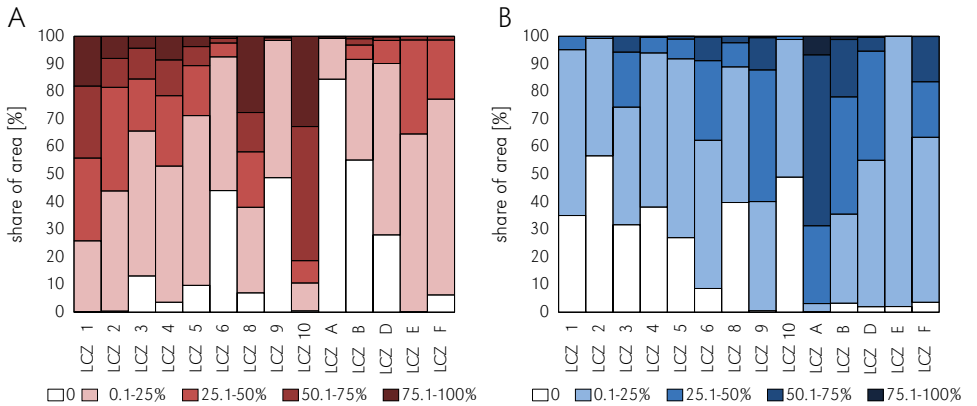

Figure 6. Local Climate Zones in the research area, divided by the frequency ranges of THS (A) and TCS (B)

Legend source: According to Demuzere et al. (2022)

trees'. At the same time, sporadic occurrences were found across other environmental types, as well as in categories 'LCZ 5 Open midrise' and 'LCZ 3 Compact lowrise'. In contrast, the most frequent effect was primarily associated with the 'LCZ 10 Heavy Industry' category. When analysing the distribution of the phenomenon from the perspective of participation in frequency ranges, 'LCZ 8 Large lowrise' dominated. 'LCZ A Dense trees' had the largest proportion of areas where the THS did not occur, while remaining ranges below 50% were mainly associated with 'LCZ 5 Open midrise'.

Examining the distribution of TCS, over half of the area in most types exhibited sporadic occurrences of the phenomenon (Fig. 6B). 'LCZ 2 Compact midrise' had the largest proportion of area where the effect was absent, while 'LCZ 9 Sparsely built' was notable for rare occurrences. Frequent occurrences dominated the surface only in the case of 'LCZ A Dense trees'. Focusing on the contribution of individual LCZs within the frequency ranges, a clear dominance of the surface occupied by 'LCZ A Dense trees' was observed in the most frequent ranges of TCS. Conversely, 'Open midrise' primarily occupied the area with the lowest frequency or absence of the effect.

Site-specific correlation analysis of the frequency of occurrence of THCS with spatial development indicators revealed the existence of urban morphology factors shaping local surface temperature extremes (Tab. 2). Firstly, a very strong negative correlation was confirmed between TCS and THS frequencies. Then, the analysis revealed a strong positive correlation of THS with FAR, a strong negative correlation with RBVA and DC, and a moderate positive correlation with BCR. The relationship of BH_{mean} and BH_{max} with THS was not statistically significant. For the TCS effect, a statistically significant, very strong negative correlation was observed between the occurrence of the phenomenon and both FAR and BCR, a strong positive correlation with RBVA and DC, and a strong negative correlation with both BH_{mean} and BH_{max}.

The cluster analysis conducted in the next step based on the frequency of THCS revealed three groups differing in the frequency of THS and TCS, land cover, and spatial development. The first cluster (5.8 distance) had the highest average TCS frequency and the lowest THS frequency (Tab. 3). It was characterised by the lowest average values of FAR, BCR, BH_{mean}, and BH_{ma}, along with the highest RBVA and moderate DC. This group included the most diverse land cover categories – both types of 'Urban fabric' (111, 112), '312. Coniferous forest', and '121. Industrial or commercial units'. It was also the only group that included

Table 2. Correlation between the occurrence of thermally distinctive surface spots, spatial development indicators and thermal characteristics

	THS	TCS	FAR	BCR	RBVA	BH_{mean}	BH_{max}	DC
THS		-0.77	0.51	0.46	-0.50	0.29	0.38	-0.55
TCS	-0.77		-0.81	-0.77	0.62	-0.50	-0.59	0.54
ATavg	0.33	-0.42	0.58	0.48	-0.60	0.62	0.57	-0.68
ATmin	0.43	-0.48	0.59	0.51	-0.68	0.55	0.52	-0.68
ATmax	0.29	-0.31	0.51	0.41	-0.54	0.65	0.57	-0.66
ATmin_abs	0.14	-0.10	0.21	0.16	-0.20	0.04	0.10	-0.46
ATmax_abs	0.01	-0.15	0.05	0.01	-0.02	0.27	0.17	0.16

Intense blue – a very strong negative; blue – a strong negative; light blue – a moderate negative; red – a strong positive; light red – a moderate positive; grey – no significant correlation.

Table 3. Spatial characteristics of clusters with different THS and TCS frequencies (%)

No.	Members	Centroid TCS	Centroid THS	FAR	BCR	RBVA	BH_{mean}	BH_{max}	DC	CLC	LCZ
1	6	42.1	3.4	0.2	5.9	73.5	9.4	15.7	7.6	111, 112, 121, 312	4, 5, 6, A, B, D
2	7	12.0	6.2	0.6	16.3	52.6	13.2	21.6	9.7	112, 121	5, 9, B
3	8	4.3	41.3	1.2	23.8	31.0	15.1	30.1	4.2	111, 112	2, 4, 5

'LCZ D Low Plants', 'LCZ A Dense Trees', and 'LCZ 6 Open lowrise' areas according to LCZ types. The second cluster (4.4 distance) exhibited moderate THS and TCS frequencies and average values for all spatial development indicators except for the greatest DC. This group encompassed '112. Discontinuous urban fabric' and '121. Industrial or commercial units' and was the only one that included 'LCZ 9 Sparsely Built' type. The highest frequency of THS, the lowest frequency of TCS, the smallest RBVA and DC, and the highest values of the remaining indicators characterised the third cluster (7.7 distance). This group's land cover included both types of 'Urban fabric' (111, 112), and it was the only cluster where 'LCZ 2 Compact Midrise' areas were found.

Relationship between the thermal surface anomalies and air temperature conditions

Site-specific air temperature analysis revealed no significant correlations between THCS frequencies and most annual thermal characteristics, except for a moderate negative correlation between TCS and AT_{min}. More significant correlations were found between thermal characteristics and spatial development indicators, especially DC, although these aspects were not the focus of this paper.

Annual and diurnal AT variability was analysed across measurement site clusters to identify air temperature patterns associated with the THCS (Tab. 4). Cluster 1, with the lowest THS and highest TCS frequency, exhibited the most moderate thermal conditions annually, except for the highest AT_{abs_max}. Sites in this group were warmer annually and during summer from sunrise (6:00) until late afternoon (17:00) and throughout the day in winter. However, the standard deviation was the largest, which could have influenced the specific values. Cluster 2, with moderate THS and TCS frequencies, had the lowest values across all annual characteristics except a moderate AT_{abs_max}. This was due to generally lower annual air temperature values,

Table 4. Thermal conditions in clusters with different THS and TCS frequencies

A. Annual thermal characteristics

No.	AT_{avg}		AT_{min}		AT_{max}		AT_{abs_min}		AT_{abs_max}	
	avg	σ	avg	σ	avg	σ	min	σ	max	σ
1	9.7	0.5	9.3	0.5	10.1	0.5	-27.3	3.7	43.6	2.6
2	9.5	0.4	9.2	0.4	9.9	0.4	-28.6	2.2	42.0	1.4
3	9.9	0.2	9.6	0.2	10.2	0.2	-23.1	1.0	39.4	0.9

B. Daily thermal regime (average for each hour from 1 to 24) during a year (I-XII), summer (VI-VII) and winter (XII-II)

Hour	1			2			3		
	I-XII	VI-VIII	XII-II	I-XII	VI-VIII	XII-II	I-XII	VI-VIII	XII-II
1	7.2	15.3	-1.3	7.2	15.6	-1.9	8.2	16.9	-1.4
2	6.9	14.9	-1.4	6.9	15.2	-2.0	7.9	16.5	-1.5
3	6.7	14.6	-1.4	6.7	14.9	-2.1	7.6	16.1	-1.6
4	6.8	14.9	-1.5	6.6	14.9	-2.2	7.5	16.1	-1.7
5	7.2	16.1	-1.5	6.9	15.7	-2.2	7.6	16.6	-1.8
6	8.1	17.8	-1.5	7.6	17.2	-2.2	8.1	17.7	-1.8
7	9.2	19.4	-1.4	8.7	19.1	-2.2	9.0	19.1	-1.7
8	10.4	20.9	-1.0	9.9	20.8	-1.8	10.0	20.6	-1.5
9	11.6	22.3	-0.4	11.1	22.1	-1.2	11.1	21.9	-1.0
10	12.6	23.3	0.3	12.1	23.2	-0.5	11.9	22.7	-0.4
11	13.3	24.1	0.9	12.8	24.0	0.1	12.6	23.4	0.1
12	13.8	24.8	1.3	13.4	24.5	0.5	13.1	24.0	0.5
13	14.1	25.2	1.4	13.5	24.6	0.7	13.4	24.3	0.7
14	14.0	25.3	1.2	13.5	24.7	0.5	13.4	24.3	0.6
15	13.6	24.9	0.8	13.1	24.4	0.2	13.1	23.9	0.4
16	12.9	24.1	0.4	12.4	23.7	-0.2	12.6	23.4	0.2
17	12.0	23.2	0.0	11.6	22.7	-0.5	12.0	22.7	-0.1
18	11.0	21.7	-0.3	10.8	21.4	-0.8	11.4	21.8	-0.3
19	10.0	19.8	-0.4	9.9	19.9	-1.0	10.7	20.8	-0.5
20	9.2	18.3	-0.6	9.2	18.6	-1.1	10.2	19.9	-0.6
21	8.6	17.4	-0.7	8.7	17.8	-1.3	9.7	19.1	-0.8
22	8.2	16.8	-0.9	8.2	17.1	-1.4	9.3	18.5	-1.0
23	7.8	16.2	-1.0	7.8	16.6	-1.6	8.9	17.9	-1.1
24	7.5	15.7	-1.1	7.5	16.1	-1.7	8.5	17.4	-1.2

Red – the highest values; Blue – the lowest values in a given hour.

particularly at night, including winter days and hours around sunrise and sunset in summer. Cluster 3, with the highest THS and lowest TCS frequencies, displayed the highest average annual air temperature values, except for AT_{abs_max}, which was the weakest among the groups. This cluster experienced significantly higher nighttime AT values annually and in summer, while daytime AT was lower or moderate in winter.

Annually, the most significant cumulative AT difference was observed between Cluster 1 and 3 (15.7°C). The maximum difference between Cluster 1 and 2 was 0.6°C at 13:00, corresponding to solar noon and the rapid intensification of thermal contrasts in different parts of the city. The difference between Cluster 2 and 3 and between Cluster 1 and 3 reached 1.1°C after 20:00, when cooling intensified following sunset. Similar observations were made for the summer season when the cumulative difference between Cluster 1 and 3 reached 23.2°C. The maximum hourly differences were 0.6°C (Clusters 1-2), 1.4°C (Clusters 2-3), and 1.7°C (Clusters 1-3). The winter season exhibited a slightly different thermal regime. The most considerable cumulative difference was 15.8°C, occurring between Cluster 1 and 2. The maximum difference between Cluster 1 and 2 was 0.8°C, observed from sunrise to noon, while for Cluster 1 and 3, it occurred outside daylight hours, and for Cluster 2 and 3, it was closest to noon. These diurnal AT differences between clusters varying in THS and TCS frequencies may explain the lack of correlation observed in year-round values.

Discussion

This paper comprehensively assessed the distribution of thermally distinctive surface areas in the context of land cover, spatial development, and associated air temperature patterns. This type of multi-aspect approach combining many sources made it possible to fill the research gap due to the lack of such studies on local thermal extremes not only in Warsaw, Poland or this climate zone but is also complementary to the few studies conducted for THCS in urban areas around the world (Guerri et al., 2022; Hussain et al., 2023; Naserikia et al., 2023). The comparability of results and easy replication was ensured by the spatial autocorrelation analysis for satellite data and by open access land cover and spatial development materials.

Significant variability in the frequency of THCS across different land cover types was observed in Warsaw during the research period, which aligns with the findings of various publications (Guerri et al., 2021; Středová et al., 2021; Liu et al., 2022; Gupta, 2024). Moreover, most land cover types or local climate zones exhibit the presence of both THS and TCS over more than half of their area, albeit with differing frequencies. The results indicate that THCS are not exclusively associated with the types of land cover they are most commonly linked to – TCS is not only related to green spaces but also occurs in densely built-up areas, within transportation infrastructure and industrial zones. Conversely, THS can be found in forested areas. The reasons are the unique physical properties of each location and their differences during a day or season.

The results may also be influenced by the resolution of satellite imagery, thermal anisotropy and the classification method of land cover types (Geletič et al., 2016; Krayenhoff & Voogt, 2016; Demuzere et al., 2022). Although widely used datasets with established protocols and high accuracy were selected, the generalisation applied in CORINE Land Cover 2018 and Global Map of Local Climate Zones may affect the precision of land classification, particularly in areas with complex spatial structures (Cheval et al., 2020; Demuzere et al., 2022; Copernicus Land Monitoring Service, accessed: 3.09.2024). However, these two datasets differ in their approach: CLC has a higher geometric resolution but a larger minimum mapping unit, whereas the Global map of LCZ has a lower geometric resolution but a smaller minimum mapping unit. As a result, CLC-based analysis provides a more detailed spatial representation. Still, it may generalise land cover types over larger areas, while LCZ analysis captures broader urban patterns but at a coarser spatial scale. Although more precise land cover databases exist (i.a. Urban Atlas), the CLC dataset was also selected due to its availability for reference year 2000, for consistent historical comparison within the study framework, to limit errors resulting from changes in the build-up environment. To address the challenges,

it is advisable not to rely on a single source or classification but to combine various land cover datasets at different scales of analysis to enhance accuracy and reliability.

The occurrence of THS is most often associated with large, compact build-up areas, usually serving an industrial and commercial function (Guerri et al., 2022; Hidalgo-García & Arco-Díaz, 2022). Moreover, an increase in developed areas, greater bare soil coverage, and a reduction in green spaces and water bodies lead to a rise in LST, intensification of the THS effect and, even more notably, a decline in TCS (Sharma et al., 2021; Hussain et al., 2023). The observed strong impact of buildings is most often associated with indicators considering horizontal dimensions, while those parametrising their height typically have weaker or more complex correlations (Huang & Wang, 2019; Zhao et al., 2023). In this study, the building height-based indicators correlated the lowest with the occurrence of TCS and were not statistically significantly associated with THS. On the other hand, FAR shows a much more substantial impact, as it reflects 3D urban morphology. The reason may be changes in air circulation, thermal radiation transfer, or the creation of shadows (Grimmond, 2007; Yuan et al., 2021). These effects vary depending on the season, time of day, and exposure, resulting in higher LST among low-rise, high-density built-up areas and lower LST in high-rise, low-density parts of the city. The spatial arrangement and 2D/3D morphology with their specific thermal properties lead to spots within artificial urban zones where THS are rare and TCS are frequent. This pattern is evident in the CLC classification and the more detailed LCZ typology, which captures the diversity of building geometry. Furthermore, urban areas differ in albedo, thermal properties of building materials and presence of small features with distinct surface temperatures, such as solar panels, condenser units or green roofs (Matias & Lopes, 2020; Guerri et al., 2021; Ramani et al., 2024). However, it should be emphasized that urban morphology also influences thermal anisotropy, which means that with increasing building height-to-width ratio, surface temperature variation in the city may be overestimated (Krayenhoff & Voogt, 2016).

Current knowledge indicates that TCS is primarily associated with vegetation and water areas (Guerri et al., 2021; Hussain et al., 2023; Kuchcik & Czarnecka, 2023). This is confirmed by the correlation with RBVA conducted in this study and many other studies based on different indicators related to vegetation (Jamei et al., 2019; Guerri et al., 2021). However, sufficiently large vegetation coverage is essential for urban parks to effectively influence LST and create zones that are noticeably cooler than their surroundings (Aram et al., 2019). This can be compromised by extensive areas covered by sidewalks or buildings that are part of the park's infrastructure or simply by the small size of the green space itself. Moreover, it is not only the presence of green areas that is significant but also the type of vegetation, their configuration, height, density structure, shape and surroundings or other landscape characteristics parameterised by metrics, such as mean patch size or edge density (Greene & Kedron, 2018; Geletič et al., 2019; Yuan et al., 2021; Liu et al., 2022). This conclusion is also evident when considering the variation in the occurrence of effects across different natural LCZ types i.e. THS is much more common on 'LCZ D low plants' than in areas densely covered with trees. In specific weather conditions, time of day or season, green areas may have higher LST, for example, due to differences in shading, condition of the vegetation, presence of an irrigation system and the thermal properties of the substrate (Chang & Li, 2014; Walawender et al., 2014; Geletič et al., 2019). All these factors may be the cause of less frequent occurrence of TCS or the presence of THS in areas classified as urban greenery or even forest.

Numerous studies have shown a statistically significant positive correlation between LST and AT, though this relationship weakens with increasing urbanisation (Gawuć et al., 2020). It varies by the season and time of day, being the weakest during winter days and the

strongest during summer, especially at night, when discrepancies are more pronounced (Grigoraș & Urițescu, 2018; Cao et al., 2021; Naserikia et al., 2023). Moreover, the relationship between LST and AT depends on time and space, varying in the distance from the ocean or urban morphology. A significant difference in values within dense built-up areas and a slight difference in the natural LCZ classes, especially in dense trees, are observed. This study indicated weak or non-existent statistically significant correlations between the frequency of occurrence of THCS and AT characteristics. It should be emphasised that this relation did not occur, even though spatial development indicators and DC were correlated with the frequencies of thermally distinctive surface spots and the values of annual AT characteristics. Similar observations can be found in the literature, where it is noted that despite the statistically significant relationship between LST and AT, the spatial distribution of their highest and lowest values is not the same (Cao et al., 2021; Středová et al., 2021). Although the detected THCS were not concerned with only one season of the year, seasonal differences in daily thermal regimes between the phenomena' frequency clusters were observed. However, the lowest AT values did not always correspond to the least frequent THS and the most frequent TCS, nor did the highest AT values consistently align with the most frequent THS and the least frequent TCS, sometimes showing inverse relationships. This may be due to the significant differences in diurnal regimes between clusters, which are strongly influenced by solar noon, the warming of various surfaces after sunrise, and cooling after sunset.

LST data is widely used in urban climate research, enabling large-scale studies and global comparability. In contrast, while adhering to WMO standards, the most commonly available AT data from synoptic stations often lack suitability for local studies due to limited coverage and non-representative locations (Sheng et al., 2017). It is important to emphasise that substituting AT with LST due to these limitations is not appropriate, especially when discussing urban climate adaptation plans, as confirmed by this study and prior research (Coutts et al., 2016; Sheng et al., 2017; Naserikia et al., 2023; Květoňová et al., 2024). LST does not fully reflect thermal conditions at the pedestrian level, particularly in dense urban areas with sparse greenery and heated rooftops. To address these limitations, research on local extremes in urban areas often combines approaches based on satellite images with weather station data from local monitoring networks (Cao et al., 2021) or crowdsourcing (Naserikia et al., 2023); however, their spatial resolution or quality may be deficient as well. While the extraction of AT from satellite imagery – particularly using complex models that account for variations depending on the land cover type – represents a promising approach, these methods remain subject to considerable limitations and require further development (Manoli et al., 2020; Martilli et al., 2020; Guo et al., 2024). An alternative option could be high-resolution gridded climate datasets, though their quality and accuracy depend on the input data (Cheval et al., 2020). However, their extensive use in studies on THCS has not been widely observed. Combining LST with in-situ AT offers significant potential to improve data quality. The results of such research can be used as input for models simulating and predicting thermal conditions in areas identified as THS or TCS in specific climate zones. Nonetheless, one must remain aware of the considerable limitations inherent in these methods, particularly in the context of human-oriented research, which should be supplemented with information that better describes outdoor thermal comfort (Jin et al., 2022; Geletič et al., 2023; Anders et al., 2025). Such insights enhance urban climate understanding and assist planners in creating thermally comfortable spaces for residents, even under burdensome thermal conditions.

Conclusions

This study examined the spatial distribution of thermal hot and cold spots in Warsaw from

2002 to 2018, highlighting their complex relationship with land cover, urban morphology and air temperature regimes. The results indicate that THCS are not solely linked to their expected land cover types or local climate zones. Instead, their occurrence is shaped by highly diverse urban settings. Although no significant correlation was found between the frequency of land surface thermal anomalies and annual air temperature averages, the study reveals that THCS exhibit distinct diurnal thermal regimes that vary seasonally.

The findings of this paper have important implications for urban planning and climate resilience strategies. A key conclusion is that relying solely on LST as an indicator of urban thermal conditions may lead to misinterpretations, as it does not always correspond with actual air temperature variations at the pedestrian level. Instead, a comprehensive approach integrating LST images, AT measurements and spatial development indicators offers a more reliable basis for simulation models and then planning more effective mitigation measures.

Further research should explore the areas where THCS persist throughout the year, especially less explored TCS that are not limited to green spaces. Additionally, a more detailed assessment of their microclimatic properties, including bioclimatic conditions, could provide valuable insights into the mechanisms driving local temperature variations and thermal comfort.

Acknowledgements

I would like to express my sincere thanks to my supervisors, Prof Magdalena Kuchcik and Dr Katarzyna Lindner-Cendrowska, for their invaluable support in the development of this research work. I also sincerely thank the authors of the datasets for providing the following data for this study:

- Land surface temperature maps from the final study defining the state of the ecosystem of the capital city of Warsaw in the context of climate change, prepared for the Foundation Institute for Sustainable Development as part of the LIFE_ADAPTCITY_PL project by the team of the Institute of Geodesy and Cartography under the supervision of Prof Katarzyna Dąbrowska-Zielińska, consisting of Dr Radosław Gurdak, Patryk Grzybowski, Damian Olszewski. The LIFE_ADAPTCITY_PL project was co-financed from the LIFE financial instrument of the European Commission and the National Fund for Environmental Protection and Water Management.
- Air temperature data from the air temperature/humidity monitoring network of the Climate Research Department Institute of Geography and Spatial Organization Polish Academy of Science consisting of a team led by Prof Magdalena Kuchcik.

Editors' note:
Unless otherwise stated, the sources of tables and figures are the author's, on the basis of their own research.

References

Ai, X., Zheng, X., Zhang, Y., Liu, Y., Ou, X., Xia, C., & Liu, L. (2024). Climate and land use changes impact the trajectories of ecosystem service bundles in an urban agglomeration: Intricate interaction trends and driver identification under SSP-RCP scenarios. *Science of The Total Environment*, *944*. https://doi.org/10.1016/j.scitotenv.2024.173828

Anders, J., Schubert, S., Maronga, B., & Salim, M. (2025). Simplifying heat stress assessment: Evaluating meteorological variables as single indicators of outdoor thermal comfort in urban environments. *Building and Environment*, *274*. https://doi.org/10.1016/j.buildenv.2025.112658

Aram, F., Higueras García, E., Solgi, E., & Mansournia, S. (2019). Urban green space cooling effect in cities. *Heliyon*, *5*(4). https://doi.org/10.1016/j.heliyon.2019.e01339

Cao, J., Zhou, W., Zheng, Z., Ren, T., & Wang, W. (2021). Within-city spatial and temporal heterogeneity of air temperature and its relationship with land surface temperature. *Landscape and Urban Planning*, *206*. https://doi.org/10.1016/j.landurbplan.2020.103979

Chang, C.-R., & Li, M.-H. (2014). Effects of urban parks on the local urban thermal environment. *Urban Forestry & Urban Greening*, *13*(4), 672-681. https://doi.org/10.1016/j.ufug.2014.08.001

Cheval, S., Micu, D., Dumitrescu, A., Irimescu, A., Frighenciu, M., Iojă, C., Tudose, N. C., Davidescu, Ș., & Antonescu, B. (2020). Meteorological and Ancillary Data Resources for Climate Research in Urban Areas. *Climate*, *8*(3), 37. https://doi.org/10.3390/cli8030037

Chief Inspectorate for Environmental Protection. (accessed: 1.05.2024-a). Corine Land Cover 2018 [Dataset]. https://clc.gios.gov.pl/index.php/clc-2018/udostepnianie

Chief Inspectorate for Environmental Protection. (accessed: 1.08.2024-b). Corrected database CORINE Land Cover 2000 [Dataset]. https://clc.gios.gov.pl/index.php/clc-2006/udostepnianie

Copernicus Land Monitoring Service. (accessed: 3.09.2024). CORINE Land Cover. https://land.copernicus.eu/en/products/corine-land-cover

Coutts, A. M., Harris, R. J., Phan, T., Livesley, S. J., Williams, N. S. G., & Tapper, N. J. (2016). Thermal infrared remote sensing of urban heat: Hotspots, vegetation, and an assessment of techniques for use in urban planning. *Remote Sensing of Environment*, *186*, 637-651. https://doi.org/10.1016/j.rse.2016.09.007

Czarnecka, K., Kuchcik, M., & Baranowski, J. (2024). Spatial development indicators as a tool to determine thermal conditions in an urban environment. *Sustainable Cities and Society*, *100*. https://doi.org/10.1016/j.scs.2023.105014

Dąbrowska-Zielińska, K., Gurdak, R., Grzybowski, P., & Olszewski, D. (2019). *Opracowanie końcowe określające stan ekosystemu m.st. Warszawy w kontekście zmian klimatu w ramach projektu LIFE_ADAPTCTY_PL*. Warsaw: Institute of Geodesy and Cartography, The Remote Sensing Center.

Dąbrowska-Zielińska, K., Hościło, A., Tomaszewska, M., & Kiryła, W. (2015). *LIFE ADAPTCITY PL – Przygotowanie strategii adaptacji do zmian klimatu miasta metropolitarnego przy wykorzystaniu mapy klimatycznej i partycypacji społecznych. Sprawozdanie z realizacji projektu*. Warsaw: Institute of Geodesy and Cartography, The Remote Sensing Center.

Demuzere, M., Kittner, J., Martilli, A., Mills, G., Moede, C., Stewart, I. D., van Vliet, J., & Bechtel, B. (2022). A global map of local climate zones to support earth system modelling and urban-scale environmental science. *Earth System Science Data*, *14*(8), 3835-3873. https://doi.org/10.5194/essd-14-3835-2022

Demuzere, M., Kittner, J., Martilli, A., Mills, G., Moede, C., Stewart, I. D., Vliet, J. van, & Bechtel, B. (2023). Global map of Local Climate Zones (3.0.0) (Version 3.0.0) [Dataset]. Zenodo. https://doi.org/10.5281/zenodo.8419340

Feyisa, G. L., Meilby, H., Darrel Jenerette, G., & Pauliet, S. (2016). Locally optimized separability enhancement indices for urban land cover mapping: Exploring thermal environmental consequences of rapid urbanization in Addis Ababa, Ethiopia. *Remote Sensing of Environment*, *175*, 14-31. https://doi.org/10.1016/j.rse.2015.12.026

Gawuć, L., Jefimow, M., Szymankiewicz, K., Kuchcik, M., Sattari, A., & Strużewska, J. (2020). Statistical modeling of urban heat island intensity in Warsaw, Poland using simultaneous air and surface temperature observations. *IEEE Journal of Selected Topics in Applied Earth Observations and Remote Sensing*, *13*, 2716-2728. https://doi.org/10.1109/JSTARS.2020.2989071

Geletič, J., Lehnert, M., & Dobrovolný, P. (2016). Land surface temperature differences within local climate zones, based on two Central European cities. *Remote Sensing*, *8*(10), 788. https://doi.org/10.3390/rs8100788

Geletič, J., Lehnert, M., Resler, J., Krč, P., Bureš, M., Urban, A., & Krayenhoff, E. S. (2023). Heat exposure variations and mitigation in a densely populated neighborhood during a hot day: Towards

a people-oriented approach to urban climate management. *Building and Environment*, *242*. https://doi.org/10.1016/j.buildenv.2023.110564

Geletič, J., Lehnert, M., Savić, S., & Milošević, D. (2019). Inter-/intra-zonal seasonal variability of the surface urban heat island based on local climate zones in three central European cities. *Building and Environment*, *156*, 21-32. https://doi.org/10.1016/j.buildenv.2019.04.011

Greene, C. S., & Kedron, P. J. (2018). Beyond fractional coverage: A multilevel approach to analyzing the impact of urban tree canopy structure on surface urban heat islands. *Applied Geography*, *95*, 45-53. https://doi.org/10.1016/j.apgeog.2018.04.004

Grigoraș, G., & Urițescu, B. (2018). Spatial hotspot analysis of Bucharest's Urban Heat Island (UHI) using modis data. *Annals of Valahia University of Targoviste Geographical Series*, *18*, 14-22. https://doi.org/10.2478/avutgs-2018-0002

Grimmond, S. (2007). Urbanization and global environmental change: Local effects of urban warming. *The Geographical Journal*, *173*(1), 83-88. https://doi.org/10.1111/j.1475-4959.2007.232_3.x

Guerri, G., Crisci, A., Congedo, L., Munafò, M., & Morabito, M. (2022). A functional seasonal thermal hot-spot classification: Focus on industrial sites. *Science of The Total Environment*, *806*. https://doi.org/10.1016/j.scitotenv.2021.151383

Guerri, G., Crisci, A., Messeri, A., Congedo, L., Munafò, M., & Morabito, M. (2021). Thermal summer diurnal hot-spot analysis: The role of local urban features layers. *Remote Sensing*, *13*(3). https://doi.org/10.3390/rs13030538

Guo, Y., Unger, J., Khabibolla, A., Tian, G., He, R., Li, H., & Gál, T. (2024). Modeling urban air temperature using satellite-derived surface temperature, meteorological data, and local climate zone pattern – A case study in Szeged, Hungary. *Theoretical and Applied Climatology*, *155*(5), 3841-3859. https://doi.org/10.1007/s00704-024-04852-7

Gupta, R. K. (2024). Identifying urban hotspots and cold spots in Delhi using the biophysical landscape framework. *Ecology, Economy and Society–the INSEE Journal*, *7*. https://doi.org/10.37773/ees.v7i1.954

He, T., Zhou, R., Ma, Q., Li, C., Liu, D., Fang, X., Hu, Y., & Gao, J. (2023). Quantifying the effects of urban development intensity on the surface urban heat island across building climate zones. *Applied Geography*, *158*. https://doi.org/10.1016/j.apgeog.2023.103052

Hebbert, M. (2014). Climatology for city planning in historical perspective. *Urban Climate*, *10*, 204-215. https://doi.org/10.1016/j.uclim.2014.07.001

Hidalgo-García, D., & Arco-Díaz, J. (2022). Modeling the Surface Urban Heat Island (SUHI) to study of its relationship with variations in the thermal field and with the indices of land use in the metropolitan area of Granada (Spain). *Sustainable Cities and Society*, *87*. https://doi.org/10.1016/j.scs.2022.104166

Huang, X., & Wang, Y. (2019). Investigating the effects of 3D urban morphology on the surface urban heat island effect in urban functional zones by using high-resolution remote sensing data: A case study of Wuhan, Central China. *ISPRS Journal of Photogrammetry and Remote Sensing*, *152*, 119-131. https://doi.org/10.1016/j.isprsjprs.2019.04.010

Hussain, N., Ahmed, S. M. S., & Shumi, A. M. (2023). Remote sensing-based geostatistical hot spot analysis of Urban Heat Islands in Dhaka, Bangladesh. *Singapore Journal of Tropical Geography*, *44*(3), 438-458. https://doi.org/10.1111/sjtg.12507

Jamei, Y., Rajagopalan, P., & Sun, Q. (Chayn). (2019). Spatial structure of surface urban heat island and its relationship with vegetation and built-up areas in Melbourne, Australia. *Science of The Total Environment*, *659*, 1335-1351. https://doi.org/10.1016/j.scitotenv.2018.12.308

Jin, L., Schubert, S., Fenner, D., Salim, M. H., & Schneider, C. (2022). Estimation of mean radiant temperature in cities using an urban parameterization and building energy model within a mesoscale atmospheric model. *Meteorologische Zeitschrift*, *31*(1), 31-52. https://doi.org/10.1127/metz/2021/1091

Kleerekoper, L., van Esch, M., & Salcedo, T. B. (2012). How to make a city climate-proof, addressing the urban heat island effect. *Resources, Conservation and Recycling*, *64*, 30-38. https://doi.org/10.1016/j.resconrec.2011.06.004

Krayenhoff, E. S., & Voogt, J. A. (2016). Daytime thermal anisotropy of urban neighbourhoods: Morphological causation. *Remote Sensing*, *8*(2), 108. https://doi.org/10.3390/rs8020108

Kuchcik, M., & Czarnecka, K. (2023). A general thermal characterisation of the Vistula Valley in Warsaw. *Przegląd Geograficzny*, *95*(3). https://doi.org/10.7163/PrzG.2023.3.6

Kuchcik, M., Czarnecka, K., & Błażejczyk, K. (2024). Urban heat island in Warsaw (Poland): Current development and projections for 2050. *Urban Climate*, *55*. https://doi.org/10.1016/j.uclim.2024.101901

Květoňová, V., Pánek, J., Geletič, J., Šimáček, P., & Lehnert, M. (2024). Where is the heat threat in a city? Different perspectives on people-oriented and remote sensing methods: The case of Prague. *Heliyon*, *10*(16). https://doi.org/10.1016/j.heliyon.2024.e36101

Lehnert, M., Geletič, J., & Jurek, M. (2023). Traditional and novel approaches to studying the human thermal environment in urban areas: A critical review of the current state of the art. *Geografie*, *128*(3), 351-377. https://doi.org/10.37040/geografie.2023.012

Liu, W., Zhao, H., Sun, S., Xu, X., Huang, T., & Zhu, J. (2022). Green space cooling effect and contribution to mitigate heat island effect of surrounding communities in Beijing Metropolitan Area. *Frontiers in Public Health*, *10*. https://doi.org/10.3389/fpubh.2022.870403

Manoli, G., Fatichi, S., Schläpfer, M., Yu, K., Crowther, T. W., Meili, N., Burlando, P., Katul, G., & Zeid, E. B. (2020). Reply to Martilli et al. (2020): Summer average urban-rural surface temperature differences do not indicate the need for urban heat reduction. *OSF Preprints*. https://doi.org/10.31219/osf.io/mwpna

Martilli, A., Roth, M., Chow, W. T. L., Demuzere, M., Lipson, M., Krayenhoff, E. S., ... & Hart, M. A. (2020). Summer average urban-rural surface temperature differences do not indicate the need for urban heat reduction. *Research Collection School of Social Sciences*, Paper 3391. https://doi.org/10.31219/osf.io/8gnbf

Matias, M., & Lopes, A. (2020). Surface radiation balance of urban materials and their impact on air temperature of an urban canyon in Lisbon, Portugal. *Applied Sciences*, *10*(6). https://doi.org/10.3390/app10062193

Mavrakou, T., Polydoros, A., Cartalis, C., & Santamouris, M. (2018). Recognition of thermal hot and cold spots in urban areas in support of mitigation plans to counteract overheating: Application for Athens. *Climate*, *6*(1). https://doi.org/10.3390/cli6010016

Naserikia, M., Hart, M. A., Nazarian, N., Bechtel, B., Lipson, M., & Nice, K. A. (2023). Land surface and air temperature dynamics: The role of urban form and seasonality. *Science of The Total Environment*, *905*. https://doi.org/10.1016/j.scitotenv.2023.167306

Office of Architecture and Spatial Planning of the Capital City of Warsaw City Hall. (2018). *Atlas Ekofizjograficzny Miasta Stołecznego Warszawy*.

Oke, T. R. (1982). The energetic basis of the urban heat island. *Quarterly Journal of the Royal Meteorological Society*, *108*(455), 1-24. https://doi.org/10.1002/qj.49710845502

Oke, T. R. (2006). Towards better scientific communication in urban climate. *Theoretical and Applied Climatology*, *84*(1), 179-190. https://doi.org/10.1007/s00704-005-0153-0

Peel, M. C., Finlayson, B. L., & McMahon, T. A. (2007). Updated world map of the Köppen-Geiger climate classification. *Hydrology and Earth System Sciences*, *11*(5), 1633-1644. https://doi.org/10.5194/hess-11-1633-2007

Ramani, V., Arjunan, P., Poolla, K., & Miller, C. (2024). Semantic segmentation of longitudinal thermal images for identification of hot and cool spots in urban areas. *Building and Environment*, *249*. https://doi.org/10.1016/j.buildenv.2023.111112

Rubel, F., & Kottek, M. (2010). Observed and projected climate shifts 1901-2100 depicted by world maps of the Köppen-Geiger climate classification. *Meteorologische Zeitschrift, 19(2),* 135-141. https://doi.org/10.1127/0941-2948/2010/0430

Sameen, M. I., & Kubaisy, M. A. A. (2014). Automatic surface temperature mapping in ArcGIS using Landsat-8 TIRS and ENVI tools, case study: Al Habbaniyah Lake. *Journal of Environment and Earth Science*, *4*(12).

Sharma, R., Pradhan, L., Kumari, M., & Bhattacharya, P. (2021). Assessing urban heat islands and thermal comfort in Noida City using geospatial technology. *Urban Climate*, *35*. https://doi.org/10.1016/j.uclim.2020.100751

Sheng, L., Tang, X., You, H., Gu, Q., & Hu, H. (2017). Comparison of the urban heat island intensity quantified by using air temperature and Landsat land surface temperature in Hangzhou, China. *Ecological Indicators*, *72*, 738-746. https://doi.org/10.1016/j.ecolind.2016.09.009

Sismanidis, P., Keramitsoglou, I., & Kiranoudis, C. T. (2017). Identifying and characterizing the diurnal evolution of urban land surface temperature patterns. *2017 Joint Urban Remote Sensing Event (JURSE)*, 1-4. https://doi.org/10.1109/JURSE.2017.7924598

Smid, M., Russo, S., Costa, A. C., Granell, C., & Pebesma, E. (2019). Ranking European capitals by exposure to heat waves and cold waves. *Urban Climate*, *27*, 388-402. https://doi.org/10.1016/j.uclim.2018.12.010

Statistics Poland. (accessed: 14.08.2024). *M.st. Warszawa. Categories: Population, Territorial division. Years: 2001, 2018*. https://bdl.stat.gov.pl/bdl/dane/teryt/jednostka#

Středová, H., Chuchma, F., Rožnovský, J., & Středa, T. (2021). Local climate zones, land surface temperature and air temperature interactions: Case study of Hradec Králové, the Czech Republic. *ISPRS International Journal of Geo-Information*, *10*(10). https://doi.org/10.3390/ijgi10100704

USGS. (accessed: 31.07.2024). *Frequently Asked Questions*. https://www.usgs.gov/faqs/

Walawender, J. P., Szymanowski, M., Hajto, M. J., & Bokwa, A. (2014). Land surface temperature patterns in the urban agglomeration of Krakow (Poland) derived from Landsat-7/ETM+ data. *Pure and Applied Geophysics*, *171*(6), 913-940. https://doi.org/10.1007/s00024-013-0685-7

Yuan, B., Zhou, L., Dang, X., Sun, D., Hu, F., & Mu, H. (2021). Separate and combined effects of 3D building features and urban green space on land surface temperature. *Journal of Environmental Management*, *295*, 113116. https://doi.org/10.1016/j.jenvman.2021.113116

Zhao, K., Qi, M., Yan, X., Li, L., & Huang, X. (2023). Dynamic impact of urban built environment on land surface temperature considering spatio-temporal heterogeneity: A perspective of local climate zone. *Land*, *12*(12). https://doi.org/10.3390/land12122148

Article first received • 19 February 2025
Article accepted • 25 April 2025